Available online at www.sciencedirect.com

ScienceDirect

IFAC PapersOnline CONFERENCE PAPER ARCHIVE

IFAC PapersOnLine 58-15 (2024) 175–180

Continuous-time identification of grey-box and black-box models of an industrial oven

Davide Previtali * **Matteo Scandella** * **Leandro Pitturelli** *
Mirko Mazzoleni * **Antonio Ferramosca** * **Fabio Previdi** *

* *Department of Management, Information and Production Engineering, University of Bergamo, Dalmine, Italy.*
email: {*name.surname*}*@unibg.it*

Abstract: The design of temperature controllers is impaired by the limited accuracy of the models employed for thermal systems, which are commonly estimated from uninformative data, such as step responses, due to the restrictive experimental design connected to the long duration of the experiments. This paper focuses on modelling an industrial convection oven following different rationales. Three continuous-time models are proposed and compared: a grey-box parametric thermal network model, a black-box parametric first order lag plus time delay model, and a black-box non-parametric model based on reproducing kernel Hilbert spaces. These are all estimated and validated on step response experimental data. Lastly, the pros and cons of each model are highlighted.

Keywords: System identification and modelling, Grey-box modelling, Black-box modelling, Continuous-time system estimation, Thermal systems.

1. INTRODUCTION

Thermal systems are present in disparate industrial sectors, including industrial furnaces used for metallurgy (Zhang et al., 2014), convection ovens employed in the food industry (Ryckaert et al., 1999), temperature test chambers for environmental testing (He et al., 2014), and Heating, Ventilation and Air Conditioning (HVAC) systems in buildings (Afroz et al., 2018). The design of temperature controllers for thermal systems is typically model-based and can be particularly challenging for two main reasons. Firstly, the controlled plants are intrinsically Multiple Inputs Multiple Outputs (MIMO) systems since they are made up of several heating/cooling zones. Secondly, the derivation of accurate control-oriented models is limited by the restrictive experimental design due to the long duration of the experiments, which can take from several hours to even days. Usually, *only open-loop step responses can be carried out on thermal systems*, see e.g. He et al. (2014); Ryckaert et al. (1999); Zhang et al. (2014). Consequently, modelling complexity must be kept in check. Most often, thermal systems are described by either grey-box models, which are derived from energy balance equations but need system identification methods to estimate their parameters, or black-box models, which are purely data-driven and require no physical knowledge (Afroz et al., 2018). Among the former, the most common are thermal network models (Sidebotham, 2015). Instead, disparate black-box models are available, ranging from First Order Lag Plus time Delay (FOLPD) transfer functions to Artificial Neural Networks (ANNs), depending on the availability of data (Afroz et al., 2018).

Thermal systems are Continuous-Time (CT) systems by nature. Consequently, it can be beneficial to describe them by CT models, such as the just mentioned thermal network models and FOLPD models, for several reasons (Garnier and Young, 2012): (i) physical insights are retained, (ii) a priori knowledge, such as the relative degree of a transfer function, is preserved, and (iii) differently from Discrete-Time (DT) models, CT models do not depend on the sampling frequency. This last advantage can be particularly relevant when designing the controller for a thermal system. For example, the derived continuous-time models can be discretized for application in a Model Predictive Control (MPC) scheme, allowing the control designer to tune the sampling/execution time of the algorithm a posteriori. We can distinguish between parametric and non-parametric CT models and identification methods. Parametric models include the previously mentioned thermal network models and FOLPD transfer functions, for which the system complexity is set a priori. Typically, parametric CT models are estimated via the output-error approach, by minimizing the difference between the measured and predicted outputs in the Least Squares sense (Garnier, 2015). Instead, kernel methods provide a non-parametric CT model which constitutes an estimate of the impulse response of the system, see i.a. Pillonetto and De Nicolao (2010); Pillonetto et al. (2014); Chen (2018); Scandella et al. (2022, 2023). If needed, a parametric model can be derived from a non-parametric one via order reduction techniques, such as Loewner interpolants (Antoulas et al., 2017; Simard and Moreschini, 2023) or similar techniques.

Contributions. In this paper, we consider the problem of modelling an industrial convection oven equipped with multiple thermocouples and heat resistors. We present and compare three state-space continuous-time models for the just mentioned application. *Similarly to many thermal systems applications, the model parameters are estimated from step response experimental data.* We derive:

(1) An ad hoc Grey-Box thermal network Parametric Model (`GBPM`),

10.1016/j.ifacol.2024.08.524

(2) A Black-Box FOLPD Parametric Model (`BBPM`),
(3) A Black-Box state-space model defined as a Loewner interpolant of a Non-Parametric Model (`BBNPM`), see the method proposed by Scandella et al. (2023).

In the thermal systems literature, few works focus on comparing different models. Most often, due to the restrictive experimental design, FOLPD models are the default choice. Consequently, comparing both parametric and non-parametric, grey-box and black-box, models is particularly relevant in this context. It is worth noting that the extension to the MIMO case of the method presented by Scandella et al. (2023) is an additional contribution.

Organization. The rest of this paper is organized as follows. Section 2 presents the industrial oven under study. Then, Section 3 describes the three different models and how their parameters are estimated. Their accuracy is assessed in Section 4. Finally, Section 5 compares the proposed models, summing up their pros and cons.

Notations. We denote by $\mathbb{C}$, $\mathbb{R}$, $\mathbb{Z}$, and $\mathbb{N}$ the set of complex, real, integer, and natural numbers respectively ($0 \notin \mathbb{N}$). ι is the imaginary unit. Given $n, m \in \mathbb{N}$, $\mathbb{C}^n$ is the set of complex column vectors of dimension n while $\mathbb{C}^{n\times m}$ is the set of complex matrices of dimension $n \times m$. Furthermore, $I_n \in \mathbb{R}^{n\times n}$ is the $n \times n$ identity matrix, and $\mathrm{diag}(a_1, \dots, a_n) \in \mathbb{R}^{n\times n}$ is the diagonal matrix with entries $a_1, \dots, a_n \in \mathbb{R}$ on the main diagonal. $\mathbb{R}_{>0}$ and $\mathbb{R}_{\geq 0}$ stand for the set of positive and non-negative real numbers respectively. Given $a \in \mathbb{R}$, $\lfloor a \rfloor$ is the greatest integer less than or equal to a. Given a signal $f : \mathbb{R}_{\geq 0} \to \mathbb{R}$, $\mathcal{L}[f] : \mathbb{C} \to \mathbb{C}$ is the Laplace transform of f. The convolution between two signals $f, g : \mathbb{R}_{\geq 0} \to \mathbb{R}$ is denoted as $[g \star f](t) = \int_0^\infty g(\psi) f(t-\psi)\, d\psi$.

2. PROBLEM STATEMENT

System description. We consider an industrial convection oven employed in plastic-shrinking processes used for product wrapping, whose schematic is depicted in Fig. 1a. The oven cavity has a volume of $2.26\,\mathrm{m}^3$ and is divided into two interconnected heating zones. The heat in each zone is produced by a pair of heat resistors, located in separate compartments. The heat resistors are connected to the electrical grid by relays (one per zone), which modulate their voltages via Pulse-Width Modulation (PWM). The duty cycles of the just mentioned voltage PWM signals are the inputs for the thermal system under study. The hot air in the proximity of the heat resistors diffuses inside the oven cavity by means of four convection fans installed at the top of the oven. The air temperature inside the oven is measured by twelve equally spaced thermocouples.

For each zone $i \in \{1, 2\}$, $q_i : \mathbb{R}_{\geq 0} \to \mathbb{R}$ is the continuous-time signal (in $\frac{\mathrm{J}}{\mathrm{s}}$) of the heat flow rate produced by the heat resistors located in zone i and $u_i : \mathbb{R}_{\geq 0} \to [0, 1]$ is the duty cycle of its corresponding voltage PWM signal. Similarly, for each thermocouple $j \in \{1, \dots, 12\}$, $y_j : \mathbb{R}_{\geq 0} \to \mathbb{R}$ is its measurement (in °C). See Fig. 1a for more details about the positioning of the sensors inside the oven. We group the $n_u = 2$ inputs (duty cycles) and $n_y = 12$ outputs (temperatures) in the vector signals $\boldsymbol{u} : \mathbb{R}_{\geq 0} \to [0, 1]^{n_u}$ and $\boldsymbol{y} : \mathbb{R}_{\geq 0} \to \mathbb{R}^{n_y}$, respectively. In particular, for every $t \in \mathbb{R}_{\geq 0}$, we have $\boldsymbol{u}(t) = [u_1(t), u_2(t)]^\top$ and $\boldsymbol{y}(t) = [y_1(t), \dots, y_{12}(t)]^\top$.

Experimental setup. We have carried out three open-loop step response experiments on the industrial oven under study. We denote the data belonging to the e-th experiment, $e \in \{1, 2, 3\}$, with the superscript (e). The first two experiments are used for model estimation. In the first trial, for every $t \in \mathbb{R}_{\geq 0}$, $u_1(t) = u_1^{(1)}(t) = 0.5$ while $u_2(t) = u_2^{(1)}(t) = 0$. Vice versa, for the second experiment, $u_1(t) = u_1^{(2)}(t) = 0, u_2(t) = u_2^{(2)}(t) = 0.5$. Instead, the third experiment, during which $u_1(t) = u_1^{(3)}(t) = 0.5$ and $u_2(t) = u_2^{(3)}(t) = 0.5$, will be used to validate the quality of the estimated models in Section 4. From each trial, we collect a dataset $\mathcal{D}^{(e)} = \left\{(t_k^{(e)}, \boldsymbol{y}_k^{(e)})\right\}_{k=1}^{N^{(e)}}$ where $N^{(e)} \in \mathbb{N}$ is the length of the experiment, $t_k^{(e)} \in \mathbb{R}$ is the sampling time of the k-th observation, and $\boldsymbol{y}_k^{(e)} = \left[y_{k,1}^{(e)}, \dots, y_{k,n_y}^{(e)}\right]^\top = \boldsymbol{y}(t_k^{(e)})$ are the output measurements. The signals are measured uniformly with sampling time $\mathcal{T}_\mathrm{s} = 1\,\mathrm{s}$, i.e. $t_k^{(e)} = (k-1)\mathcal{T}_\mathrm{s}$ for every $k \in \left\{1, \dots, N^{(e)}\right\}$.

3. MODELLING AND IDENTIFICATION

This Section is devoted to the derivation of continuous-time state-space models for the industrial oven under study. All models are estimated from the available data described in Section 2.

3.1 Grey-Box thermal network Parametric Model (`GBPM`)

Following the thermal-electrical analogy (Sidebotham, 2015), we describe the relationship between the heat produced by the heat resistors and the temperatures measured by the twelve thermocouples using the electro-equivalent thermal circuit presented in Fig. 1b. For each zone $i \in \{1, 2\}$, location $k \in \{1, 2, 3\}$, $k' \in \{1, 2\}$, and side $d \in \{\mathrm{l}, \mathrm{r}\}$ (l: left, r: right), we define:

- $R_i^{(k,d)} \in \mathbb{R}_{>0}$ (in $\frac{^\circ\mathrm{C}}{\mathrm{J}}\mathrm{s}$) is the thermal resistance between the oven walls of zone i, location k, side d, and the ambient;
- $R_{\mathrm{T}_i}^{(k',d)} \in \mathbb{R}_{>0}$ (in $\frac{^\circ\mathrm{C}}{\mathrm{J}}\mathrm{s}$) is the thermal resistance related to the transfer of heat between two locations of zone i, side d;
- $R_{\mathrm{T}_{12}}^{(d)} \in \mathbb{R}_{>0}$ (in $\frac{^\circ\mathrm{C}}{\mathrm{J}}\mathrm{s}$) is the thermal resistance related to the transfer of heat between the two zones of the oven, for what concerns side d;
- $R_{\mathrm{T}_{\mathrm{lr}}} \in \mathbb{R}_{>0}$ (in $\frac{^\circ\mathrm{C}}{\mathrm{J}}\mathrm{s}$) is the thermal resistance related to the transfer of heat between the left and the right side of the oven cavity;
- $C_\mathrm{z} \in \mathbb{R}_{>0}$ (in $\frac{\mathrm{J}}{^\circ\mathrm{C}}$) is the thermal capacitance of the air in each zone/location/side of the oven cavity, which all have the same volume.
- $T_\mathrm{a} : \mathbb{R}_{\geq 0} \to \mathbb{R}$ is the ambient temperature as a function of time. It is assumed to be constant, i.e. $T_\mathrm{a}(t) = \bar{T}_\mathrm{a} \in \mathbb{R}$ (in °C), for every $t \in \mathbb{R}_{\geq 0}$.

The relationship between each temperature and the heat flow rates can be readily derived from the circuit in Fig. 1b, leading to the following system of linear differential equations (Sidebotham, 2015):

$$\dot{\boldsymbol{y}}(t) = A_{TT}\, \boldsymbol{y}(t) + B_q\, \boldsymbol{q}(t) + \boldsymbol{b}_T\, T_\mathrm{a}(t), \tag{1}$$

where $\boldsymbol{q}(t) = [q_1(t), q_2(t)]^\top$ while $A_{TT} \in \mathbb{R}^{n_y \times n_y}$, $B_q \in \mathbb{R}^{n_y \times 2}$ and $\boldsymbol{b}_T \in \mathbb{R}^{n_y}$ are matrices whose definition can

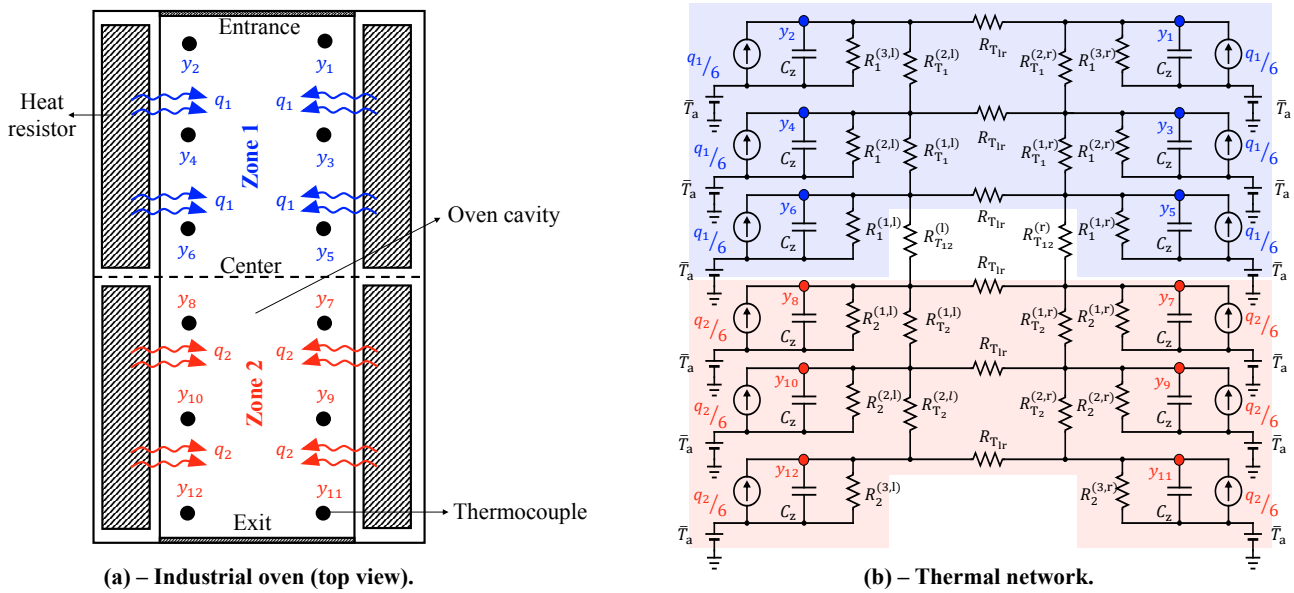

(a) – Industrial oven (top view). **(b) – Thermal network.**

Fig. 1. Schematic of the considered industrial oven and associated thermal network (zone 1 in blue, zone 2 in red).

be found from the electro-equivalent thermal circuit in Fig. 1b. Their expressions are omitted here for space reason.

The heat flow rates $\boldsymbol{q}$ in (1) are generated by the heat resistors located in the corresponding zones, which operate in pairs. We denote the voltage signals across the couples of heat resistors as $V_1, V_2 : \mathbb{R}_{\geq 0} \to \mathbb{R}$ (in V). Let $R_{\text{heat}} \in \mathbb{R}_{>0}$ (in Ω) be the resistance of a pair of heat resistors and assume that it is the same for each pair. Then, due to Joule heating, we have $q_i(t) = R_{\text{heat}}^{-1} V_i(t)^2$ for $i \in \{1, 2\}$. As pointed out in Section 2, the voltages V_1 and V_2 are PWM signals with period $\mathcal{T}_{\text{P}} \in \mathbb{R}_{>0}$ and duty cycles $u_1(t)$ and $u_2(t)$, respectively, for every $t \in \mathbb{R}_{\geq 0}$. By definition, for every $i \in \{1, n_u\}$, u_i is a piecewise constant signal since

$$\forall \tilde{t} \in \mathbb{N} \cup \{0\},\ \forall t \in [\tilde{t}\,\mathcal{T}_{\text{P}}, (\tilde{t}+1)\,\mathcal{T}_{\text{P}}), \quad u_i(t) = u_i(\tilde{t}\mathcal{T}_{\text{P}}).$$

Then, assuming that the grid voltage stays constant at a value $V_{\text{g}} \in \mathbb{R}_{>0}$ (in V), we have

$$V_i(t) = f_V\left(t, u_i(t); \mathcal{T}_{\text{P}}, V_{\text{g}}\right) = \begin{cases} V_{\text{g}} & \text{if } \tilde{t}\,\mathcal{T}_P \leq t < \left[\tilde{t} + u_i(t)\right]\,\mathcal{T}_P \\ 0 & \text{otherwise} \end{cases}, \quad \tilde{t} = \left\lfloor \frac{t}{\mathcal{T}_{\text{P}}} \right\rfloor,$$

where $f_V : \mathbb{R}_{\geq 0} \times [0, 1] \times \mathbb{R}_{>0} \times \mathbb{R}_{>0} \to \mathbb{R}_{\geq 0}$ is the function describing a PWM signal. Consequently, we define the multivariable function $\boldsymbol{f}_{V_{\text{sq}}}$ as follows:

$$\boldsymbol{f}_{V_{\text{sq}}}\left(t, \boldsymbol{u}(t); \mathcal{T}_{\text{P}}, V_{\text{g}}\right) = \begin{bmatrix} f_V\left(t, u_1(t); \mathcal{T}_{\text{P}}, V_{\text{g}}\right)^2 \\ f_V\left(t, u_2(t); \mathcal{T}_{\text{P}}, V_{\text{g}}\right)^2 \end{bmatrix},$$

leading to

$$\boldsymbol{q}(t) = R_{\text{heat}}^{-1}\, \boldsymbol{f}_{V_{\text{sq}}}\left(t, \boldsymbol{u}(t); \mathcal{T}_{\text{P}}, V_{\text{g}}\right). \tag{2}$$

Finally, we model the propagation of heat from the heat resistors to the air inside the oven cavity using a first-order low-pass filter with unitary gain:

$$\forall i \in \{1, 2\}, \quad \dot{q}_i^{(\text{f})}(t) = -\tau_i^{-1}\, q_i^{(\text{f})}(t) + \tau_i^{-1}\, q_i(t) \tag{3}$$

where $q_i^{(\text{f})}$ is the filtered signal and $\tau_i \in \mathbb{R}_{>0}$ (in s) is the time constant for zone i. By combining (1), (2), and (3), we obtain the GBPM:

$$\begin{cases} \dot{\boldsymbol{q}}^{(\text{f})}(t) = A_{ff}\, \boldsymbol{q}^{(\text{f})}(t) + B_f\, \boldsymbol{f}_{V_{\text{sq}}}\left(t, \boldsymbol{u}(t); \mathcal{T}_{\text{P}}, V_{\text{g}}\right) \\ \dot{\boldsymbol{y}}(t) = A_{TT}\, \boldsymbol{y}(t) + B_q\, \boldsymbol{q}^{(\text{f})}(t) + \boldsymbol{b}_T\, T_{\text{a}}(t), \end{cases} \tag{4}$$

where $\boldsymbol{q}^{(\text{f})}(t) = [q_1^{(\text{f})}(t), q_2^{(\text{f})}(t)]^\top$, $A_{ff} = -\operatorname{diag}(\tau_1^{-1}, \tau_2^{-1}) \in \mathbb{R}^{2\times 2}$ and $B_f = -R_{\text{heat}}^{-1} A_{ff} \in \mathbb{R}^{2\times 2}$. This model has $n_x = 14$ states, i.e. $\boldsymbol{x} = [\boldsymbol{q}^{(\text{f})}, \boldsymbol{y}]^\top$, which all have physical meaning.

Identification. The thermal capacitance and the grid voltage can be readily derived from the dimensions of the oven and its nominal working conditions, resulting in $C_{\text{z}} = 231\,\frac{\text{J}}{^\circ\text{C}}$ and $V_{\text{g}} = 390\,\text{V}$. Consequently, the GBPM in (4) depends only on $n_\theta = 26$ unknown parameters, i.e. the thermal resistances $R_i^{(k,d)}, R_{\text{T}_i}^{(k',d)}, R_{\text{T}_{12}}^{(d)}, R_{\text{T}_{\text{lr}}}$ for each $i \in \{1, 2\}, k \in \{1, 2, 3\}, k' \in \{1, 2\}, d \in \{\text{l}, \text{r}\}$, the ohmic resistance R_{heat}, and the time constants τ_1 and τ_2. These are collected in the vector $\boldsymbol{\theta} \in \mathbb{R}_{>0}^{n_\theta}$ and they are estimated from the available data. In particular, we employ a simulation error approach that minimizes the difference between the available measurements and the simulated temperatures with a specific parameter vector in the Least Squares sense. More formally, we define the cost function

$$J_{\text{GBPM}}(\boldsymbol{\theta}) = \frac{1}{2} \sum_{e=1}^{2} \left[\frac{1}{N^{(e)}} \sum_{k=1}^{N^{(e)}} \left\| \boldsymbol{y}_k^{(e)} - \hat{\boldsymbol{y}}^{(e)}\left(t_k^{(e)}; \boldsymbol{\theta}\right) \right\|_2^2 \right],$$

where $\hat{\boldsymbol{y}}^{(e)}(t; \boldsymbol{\theta})$ is the output of Model (4) with parameter vector $\boldsymbol{\theta} \in \mathbb{R}_{>0}^{n_\theta}$ simulated with the input of experiment $e \in \{1, 2\}$ at time $t \in \mathbb{R}_{\geq 0}$. Due to the MIMO nature of the model in (4), cost function $J_{\text{GBPM}}(\boldsymbol{\theta})$ considers the first two experiments in the same optimization problem.

3.2 Black-Box FOLPD Parametric Model (BBPM)

Instead of relying on the physical description of the system provided in Section 3.1, in this method, we model the relationship between the inputs $\boldsymbol{u}$ and outputs $\boldsymbol{y}$ using a FOLPD transfer function. Here, we neglect the effect of the ambient temperature because we assume its contribution to the output to be constant (see Section 3.1); conse-

quently, it can be added a posteriori. For each $i \in \{1, n_u\}$ and $j \in \{1, \dots, n_y\}$, we have:

$$G_{j,i}(s) = \frac{\mathcal{L}[y_j](s)}{\mathcal{L}[u_i](s)} = \frac{\mu_{j,i}}{1 + s\tau_{j,i}} e^{-sL_{j,i}}, \tag{5}$$

where $\mu_{j,i} \in \mathbb{R}_{>0}$ is the gain (in °C), $\tau_{j,i} \in \mathbb{R}_{>0}$ is the time constant (in s), and $L_{j,i} \in \mathbb{R}_{\geq 0}$ is the input-output time delay (in s). A possible realization of its corresponding MIMO state-space model is (`BBPM`):

$$\begin{cases} v_i(t) = u_i\big(t - L_i^{(u)}\big) & i = 1, n_u \\ \dot{\boldsymbol{x}}(t) = A\boldsymbol{x}(t) + B\boldsymbol{v}(t) \\ \boldsymbol{z}(t) = C\boldsymbol{x}(t) \\ y_j(t) = z_j\big(t + L_j^{(y)}\big) & j = 1, \dots, n_y \end{cases} \tag{6}$$

where $\boldsymbol{v}(t) = [v_1(t), v_{n_u}(t)]^\top$ are the delayed inputs with associated input delays $L_1^{(u)}, L_{n_u}^{(u)} \in \mathbb{R}_{\geq 0}$, $\boldsymbol{z}(t) = [z_1(t), \dots, z_{n_y}(t)]^\top$ are the outputs before the time shift, with associated output delays $L_1^{(y)}, \dots, L_{n_y}^{(y)} \in \mathbb{R}_{\geq 0}$, and

$$A = -\operatorname{diag}\Big(\tau_{1,1}^{-1}, \dots, \tau_{n_y,1}^{-1}, \tau_{1,n_u}^{-1}, \dots, \tau_{n_y,n_u}^{-1}\Big) \in \mathbb{R}^{n_x \times n_x},$$

$$B = \begin{bmatrix} \tau_{1,1}^{-1} & \cdots & \tau_{n_y,1}^{-1} & 0 & \cdots & 0 \\ 0 & \cdots & 0 & \tau_{1,n_u}^{-1} & \cdots & \tau_{n_y,n_u}^{-1} \end{bmatrix}^\top \in \mathbb{R}^{n_x \times n_u},$$

$$C = \big[\operatorname{diag}\big(\mu_{1,1}, \dots, \mu_{n_y,1}\big) \ \operatorname{diag}\big(\mu_{1,n_u}, \dots, \mu_{n_y,n_u}\big)\big] \in \mathbb{R}^{n_y \times n_x}$$

where $n_x = n_y n_u = 24$ is the number of states for the `BBPM` in (6). Moreover, the `BBPM` in (6) is an exact realization of Model (5) if and only if

$$\forall i \in \{1, n_u\}, \forall j \in \{1, \dots, n_y\}, \quad L_{j,i} = L_j^{(y)} + L_i^{(u)}. \tag{7}$$

In practice, these conditions amount to an overdetermined system with $n_y n_u = 24$ equations and $n_y + n_u = 14$ unknows. Thus, we select an approximation of $\big\{L_j^{(y)}\big\}_{j=1}^{n_y}$ and $\big\{L_i^{(u)}\big\}_{i=1}^{n_u}$ by solving (7) via ordinary Least Squares.

Identification. Similarly to the approach explained in Section 3.1, we employ a simulation error method that minimizes the difference between the available data and the simulated measurements obtained with a specific parameter vector. Exploiting the structure of Model (6), we simplify the problem by identifying $n_y n_u$ SISO models separately, one for each couple of input and output. In particular, for each $i \in \{1, n_u\}$ and $j \in \{1, \dots, n_y\}$, $\boldsymbol{\theta}_{j,i} = [\mu_{j,i}, \tau_{j,i}, L_{j,i}]^\top \in \mathbb{R}^3_{\geq 0}$ is the parameter vector of the (j,i)-th transfer function in (5). We select $\boldsymbol{\theta}_{j,i}$ by minimizing the cost function

$$J_{\texttt{BBPM},j,i}(\boldsymbol{\theta}_{j,i}) = \sum_{k=1}^{N^{(i)}} \Big[y_{k,j}^{(i)} - \hat{y}_j^{(i)}\Big(t_k^{(i)}; \boldsymbol{\theta}_{j,i}\Big)\Big]^2$$

where $\hat{y}_j^{(i)}(t; \boldsymbol{\theta}_{j,i})$ is the output of $G_{j,i}$ in (5) with parameter vector $\boldsymbol{\theta}_{j,i}$ simulated with the input of experiment $i \in \{1, 2\}$ at time $t \in \mathbb{R}_{\geq 0}$. Then, we derive the state-space model in (6) using the $3n_y n_u = 72$ identified parameters.

3.3 Black-Box Non-Parametric Model (`BBNPM`)

As a third approach, we use the non-parametric method illustrated by Scandella et al. (2022) to estimate the SISO model between each input and output (neglecting the ambient temperature as in Section 3.2). Then, we obtain the complete MIMO model via the procedure in Scandella et al. (2023) expanded to handle MIMO models. In more details, for each $i \in \{1, n_u\}$ and $j \in \{1, \dots, n_y\}$, we estimate the impulse response $\hat{g}_{j,i} : \mathbb{R}_{\geq 0} \to \mathbb{R}$ of the model with input u_i and output y_j by solving

$$\underset{\hat{g}_{j,i} \in \mathcal{H}_{j,i}}{\operatorname{argmin}} \sum_{k=1}^{N^{(i)}} \Big(y_{k,j}^{(i)} - \big[\hat{g}_{j,i} \star u_i^{(i)}\big]\big(t_k^{(i)}\big)\Big)^2 + \sigma_{j,i} \|\hat{g}_{j,i}\|^2_{\mathcal{H}_{j,i}} \tag{8}$$

where $\mathcal{H}_{j,i}$ is the Reproducing Kernel Hilbert Space (RKHS) associated with kernel $\kappa_{j,i}$ (Aronszajn, 1950), $\|\hat{g}_{j,i}\|_{\mathcal{H}_{j,i}}$ is its norm, and $\sigma_{j,i} \in \mathbb{R}_{\geq 0}$ is a hyperparameter that regulates the complexity of the model (which needs to be tuned). Here, we propose to use the stable spline kernel $\kappa_{j,i} : \mathbb{R}_{\geq 0} \times \mathbb{R}_{\geq 0} \to \mathbb{R}$, which is defined as:

$$\kappa_{j,i}(a,b) = \lambda_{j,i} \sum_{h=0}^{p_{j,i}-1} \gamma_{p_{j,i},h} \begin{cases} e^{-\beta_{j,i}[(2p_{j,i}-h-1)a + hb]} & a \geq b \\ e^{-\beta_{j,i}[(2p_{j,i}-h-1)b + ha]} & a < b \end{cases}$$

where $\lambda_{j,i}, \beta_{j,i} \in \mathbb{R}_{\geq 0}$ and $p_{j,i} \in \mathbb{N}$ are kernel hyperparameters that need to be tuned, while

$$\gamma_{p_{j,i},h} = \frac{(-1)^{p_{j,i}+h+1}}{h!(2p_{j,i} - h - 1)!}.$$

Due to the Representer Theorem (Dinuzzo and Schölkopf, 2012), the solution of Problem (8) amounts to

$$\hat{g}_{j,i}(t) = \sum_{k=1}^{N^{(i)}} c_{j,i,k} \int_0^\infty u_i^{(i)}\big(t_k^{(i)} - \psi\big) \kappa_{j,i}(t, \psi)\, d\psi, \tag{9}$$

where $\boldsymbol{c}_{j,i} = \big[c_{j,i,1}, \dots, c_{j,i,N^{(i)}}\big]^\top \in \mathbb{R}^{N^{(i)}}$ is the solution of the linear system

$$O_{j,i}\big(O_{j,i} + \sigma_{j,i} I_{N^{(i)}}\big)\, \boldsymbol{c}_{j,i} = O_{j,i} \bar{\boldsymbol{y}}_j$$

with $\bar{\boldsymbol{y}}_j = \big[y_{1,j}^{(i)}, \dots, y_{N^{(i)},j}^{(i)}\big]^\top \in \mathbb{R}^{N^{(i)}}$ and $O_{j,i} \in \mathbb{R}^{N^{(i)} \times N^{(i)}}$ being a matrix whose (k,k')-th entry is

$$\int_0^\infty \int_0^\infty u_i^{(i)}\Big(t_k^{(i)} - \xi\Big)\, u_i^{(i)}\Big(t_{k'}^{(i)} - \psi\Big)\, \kappa_{j,i}(\xi, \psi)\, d\psi\, d\xi. \tag{10}$$

The hyperparameters $\boldsymbol{\theta}_{j,i} = [\lambda_{j,i}, \beta_{j,i}, p_{j,i}, \sigma_{j,i}]^\top$ can be found using the empirical Bayes method (Rasmussen and Williams, 2006, Sec. 5.4.1). In particular, they are selected by minimizing the cost function

$$J_{\texttt{BBNPM},j,i}(\boldsymbol{\theta}_{j,i}) = \bar{\boldsymbol{y}}_j^\top \big(O_{j,i} + \sigma_{j,i} I_{N^{(i)}}\big)^{-1} \bar{\boldsymbol{y}}_j + \\ + \ln\det\big(O_{j,i} + \sigma_{j,i} I_{N^{(i)}}\big). \tag{11}$$

In total, there are $4n_y n_u = 96$ hyperparameters to estimate. The estimated model are then optimized using the method presented by Scandella et al. (2021). Finally, we can merge the $n_y n_u$ estimated impulse responses to define the MIMO transfer function $\hat{\boldsymbol{G}} : \mathbb{C} \to \mathbb{C}^{n_y \times n_u}$ of the model. In particular, we have

$$\hat{\boldsymbol{G}} = \begin{bmatrix} \mathcal{L}[\hat{g}_{1,1}] & \cdots & \mathcal{L}[\hat{g}_{n_y,1}] \\ \mathcal{L}[\hat{g}_{1,n_u}] & \cdots & \mathcal{L}[\hat{g}_{n_y,n_u}] \end{bmatrix}^\top.$$

In Scandella et al. (2022), the authors analyze this transfer function when the experiment is executed with a step input, and they derive a closed-form expression for (10). However, $\hat{\boldsymbol{G}}$ is a transcendental transfer function that does not admit a finite rational form. In this paper, we retrieve a rational form using a Loewner interpolant (Antoulas et al., 2017), as proposed by Scandella et al. (2023).

The Loewner interpolant provides an LTI model whose transfer function interpolates a set of interpolation points. In particular, we consider $2m \in \mathbb{N}$ interpolation points divided in two sets

$$\left\{\left(s_k^{(\ell)}, \boldsymbol{\ell}_k\right)\right\}_{k=1}^{m} \in \mathbb{C} \times \mathbb{C}^{n_y}, \quad \left\{\left(s_k^{(r)}, \boldsymbol{r}_k\right)\right\}_{k=1}^{m} \in \mathbb{C} \times \mathbb{C}^{n_u},$$

such that $\left\{s_k^{(\ell)}\right\}_{k=1}^{m} \cap \left\{s_k^{(r)}\right\}_{k=1}^{m} = \varnothing$. Then, we say that a model with transfer function $\check{\boldsymbol{G}} : \mathbb{C} \to \mathbb{C}^{n_y \times n_u}$ is a tangential interpolant of $\hat{\boldsymbol{G}}$ if and only if, for each $k \in \{1, \dots, m\}$,

$$\boldsymbol{\ell}_k^\top \hat{\boldsymbol{G}}\left(s_k^{(\ell)}\right) = \boldsymbol{\ell}_k^\top \check{\boldsymbol{G}}\left(s_k^{(\ell)}\right), \quad \hat{\boldsymbol{G}}\left(s_k^{(r)}\right)\boldsymbol{r}_k = \check{\boldsymbol{G}}\left(s_k^{(r)}\right)\boldsymbol{r}_k.$$

Now, a tangential interpolant of $\hat{\boldsymbol{G}}$ has transfer function

$$\check{\boldsymbol{G}}(s) = -W^{(r)}(s\mathbb{L} - \mathbb{L}_{\mathrm{s}})^{-1} W^{(\ell)}$$

where

$$W^{(r)} = \left[\hat{\boldsymbol{G}}\left(s_1^{(r)}\right)\boldsymbol{r}_1, \dots, \hat{\boldsymbol{G}}\left(s_m^{(r)}\right)\boldsymbol{r}_m\right] \in \mathbb{C}^{n_y \times m},$$

$$W^{(\ell)} = \left[\boldsymbol{\ell}_1^\top \hat{\boldsymbol{G}}\left(s_1^{(\ell)}\right), \dots, \boldsymbol{\ell}_m^\top \hat{\boldsymbol{G}}\left(s_m^{(\ell)}\right)\right]^\top \in \mathbb{C}^{m \times n_u},$$

and $\mathbb{L}, \mathbb{L}_{\mathrm{s}} \in \mathbb{C}^{m \times m}$ are, respectively, the solutions of the Sylvester equations

$$S^{(\ell)}\mathbb{L} - \mathbb{L}S^{(r)} = W^{(\ell)}R - LW^{(r)}$$

$$S^{(\ell)}\mathbb{L}_{\mathrm{s}} - \mathbb{L}_{\mathrm{s}}S^{(r)} = S^{(\ell)}W^{(\ell)}R - LW^{(r)}S^{(r)}$$

in which $R = [\boldsymbol{r}_1, \dots, \boldsymbol{r}_m] \in \mathbb{R}^{n_u \times m}$, $L = [\boldsymbol{\ell}_1, \dots, \boldsymbol{\ell}_m]^\top \in \mathbb{R}^{m \times n_y}$, and $S^{(\ell)}, S^{(r)} \in \mathbb{R}^{m \times m}$ are matrices whose eigenvalues are $\left\{s_k^{(\ell)}\right\}_{k=1}^{m}$ and $\left\{s_k^{(r)}\right\}_{k=1}^{m}$, respectively. In general, this approximant cannot be applied as is because it may generate complex outputs and because it may be unstable. Furthermore, the matrices $\mathbb{L}$ and $\mathbb{L}_{\mathrm{s}}$ can be singular. Hence, the rational model may not be in minimum realization. These problems were solved in Scandella et al. (2023) by proposing a real and asymptotically stable interpolant in minimum realization. In particular, the reduced model admits the following state-space representation (`BBNPM`)

$$\begin{cases} \check{E}\dot{\boldsymbol{x}}(t) = \check{A}\boldsymbol{x}(t) + \check{B}\boldsymbol{u}(t) \\ \boldsymbol{y}(t) = \check{C}\boldsymbol{x}(t) \end{cases}$$

where $\check{E}, \check{A} \in \mathbb{R}^{n_x \times n_x}$, $\check{B} \in \mathbb{R}^{n_x \times n_u}$, $\check{C} \in \mathbb{R}^{n_y \times n_x}$ and $n_x \in \mathbb{N}$ is the order of the model. It is worth noting that $n_x \leq m$. Thus, the order of the estimated model is not set a priori: it can be modified by changing the number of interpolation points.

For comparison purposes, we employ three different sets of interpolation points with $m = 50$, $m = 30$ and $m = 20$, respectively. In all the three cases, we define the set of interpolation point as $\{\omega_k, \iota\omega_k, -\iota\omega_k, (1+\iota)\omega_k, (1-\iota)\omega_k\}_{k=1}^{0.4m}$ where $\omega_1 = 10^{-4}$, $\omega_{0.4m} = 10^{-1}$ and $\ln(\omega_{k+1}) - \ln(\omega_k) = \ln(\omega_{k'+1}) - \ln(\omega_{k'})$ for every $k, k' \in \{1, \dots, 0.4m - 1\}$. In all cases, the matrices R and L are chosen randomly, and their elements are mutually independent random variables distributed according to a Normal distribution with zero mean and unitary variance. Therefore, we obtain three different estimated models:

(1) `BBNPM_42` with $m = 50$ leading to $n_x = 42$;
(2) `BBNPM_24` with $m = 30$ leading to $n_x = 24$, making its order comparable to the `BBPM` model in Section 3.2;
(3) `BBNPM_14` with $m = 20$ leading to $n_x = 14$, making its order comparable to the `GBPM` in Section 3.1.

4. EXPERIMENTAL RESULTS

We evaluate the performances of the models on the available experimental data according to the following measure of fit for each output $y_j, j \in \{1, \dots, n_y\}$:

$$\mathrm{Fit}_j^{(e)} = 1 - \sqrt{\frac{\sum_{k=1}^{N^{(e)}} \left| y_{k,j}^{(e)} - \hat{y}_j^{(e)}\left(t_k^{(e)}\right)\right|^2}{\sum_{k=1}^{N^{(e)}} \left| y_{k,j}^{(e)} - \frac{1}{N^{(e)}} \sum_{k'=1}^{N^{(e)}} y_{k',j}^{(e)}\right|^2}}, \tag{12}$$

where $\hat{y}_j^{(e)}(t)$ is the j-th output of the estimated model simulated using the input of experiment $e \in \{1, 2, 3\}$ at time $t \in \mathbb{R}_{\geq 0}$. The results are reported in Fig. 2.

We can clearly see that the `GBPM` and `BBNPM_14` (with $n_x = 14$) severely underperform on the datasets used for parameters estimation (i.e. $e = 1$ or $e = 2$) compared to those with higher orders, mostly because they fail to capture the static gains of the system (see Fig. 3). This could be due to the input choice, which is not sufficiently informative for estimation purposes, or the model order, which may be too low for describing the system under study. Clearly, it is not straightforward to increase n_x for the `GBPM` in Section 3.1 since its structure is intrinsically connected to the considered industrial oven. On the other hand, the order of the non-parametric model in Section 3.3 can be easily changed by modifying the interpolation points for Loewner reduction. In fact, that is the case for the `BBNPM_42` and `BBNPM_24` models, which are the best performing ones for $e = 1$ and $e = 2$. On estimation data, the `BBPM` model also behaves quite well, achieving fits that are only slightly lower than the aforementioned models. For what concerns the validation dataset ($e = 3$), the disparity in performances is less evident. In any case, Fig. 2 shows that `BBNPM_24` has better performances by a small margin (median-wise). Overall, when comparing models with the same order n_x (`BBNPM_24`/`BBPM` and `BBNPM_14`/`GBPM`), the non-parametric methodologies seem to outperform the others. Finally, the experimental results depicted in Fig. 2 show that, even when compared to the most complex model (i.e. the `BBNPM_42`), the `BBNPM_24` achieves the best complexity/performances trade-off.

5. DISCUSSION

This paper proposed and compared three continuous-time models for an industrial convection oven, either parametric or non-parametric, grey-box or black-box. This Section is devoted to highlighting their pros and cons. Due to the restrictive experimental design that is common to most thermal systems, only open-loop step responses are available for model estimation. The `GBPM` in Section 3.1 is derived by building an ad hoc thermal network for the system under study. Although the model has strong physical meaning and takes into account the locations at which the temperatures are measured, its derivation is quite cumbersome and requires solving a complex electrical circuit. However, its parameters are useful for designing the industrial oven itself since they give an indication on the efficiency related to the transfer of heat within the cavity and the losses towards the ambient. Unfortunately, experimental results show that simple step response tests are not suitable for the estimation of the parameters of the `GBPM`. Instead, the black-box models in Section 3.2

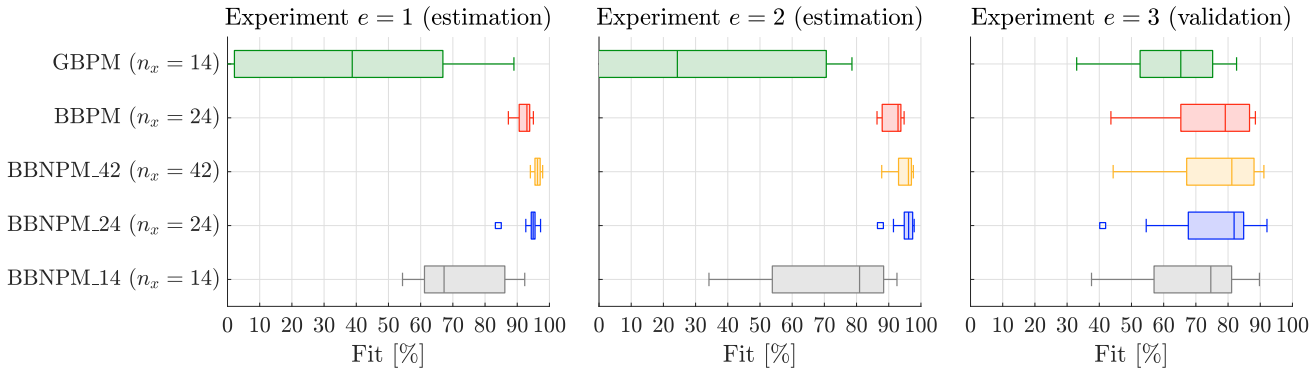

Fig. 2. Box plots of the performance index in (12) for each model and each experiment.

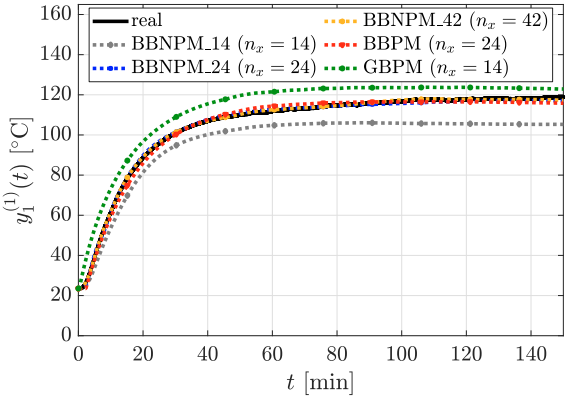

Fig. 3. Example of performances on $\mathcal{D}^{(1)}$ that highlights the shortcomings of the `GBPM` and `BBNPM_14`.

and Section 3.3 have no physical meaning but are general and easily applicable, at the cost of having more parameters. FOLPD models (Section 3.2) are commonly used when only step data is available, due to their simplicity, exhibiting satisfactory performances on the experimental data at our disposal. Analogously to the `GBPM`, the `BBPM` has a fixed order but presents input and output delays that can impair controller design. In any case, the parameters of the `BBPM` model are easily interpretable, highlighting the hottest spots within the oven (larger gains) and the time required for the heat to propagate inside the cavity (time constants/time delays). Lastly, the `BBNPM` in Section 3.3 is the most complex and least interpretable among the three, but the best performing one. Its main advantage is the possibility of setting the model order a posteriori. Moreover, step response data is not a limiting factor; in fact, there are readily available closed-form expressions for (9) and (10) in this case (Scandella et al., 2022).

REFERENCES

Afroz, Z., Shafiullah, G., Urmee, T., and Higgins, G. (2018). Modeling techniques used in building HVAC control systems: A review. *Renew. sustain. energy rev.*, 83, 64–84.

Antoulas, A.C., Lefteriu, S., Ionita, A.C., Benner, P., and Cohen, A. (2017). A tutorial introduction to the Loewner framework for model reduction. *Model Reduct. Approx.: Theory Algorithms*, 15, 335.

Aronszajn, N. (1950). Theory of reproducing kernels. *Trans. Am. math. soc.*, 68(3), 337–404.

Chen, T. (2018). On kernel design for regularized LTI system identification. *Automatica*, 90, 109–122.

Dinuzzo, F. and Schölkopf, B. (2012). The representer theorem for Hilbert spaces: a necessary and sufficient condition. In *Adv. Neural Inf. Process. Syst.*, volume 25.

Garnier, H. (2015). Direct continuous-time approaches to system identification. Overview and benefits for practical applications. *Eur. J. control*, 24, 50–62.

Garnier, H. and Young, P.C. (2012). What does continuous-time model identification have to offer? In *Proc. 16th IFAC Symp. Syst. Identif.*, volume 45, 810–815.

He, W., Xu, G., and Shen, R. (2014). Control of temperature uniformity in the temperature chamber with centrifugal acceleration. *J. Process Control*, 24(12), 1–6.

Pillonetto, G. and De Nicolao, G. (2010). A new kernel-based approach for linear system identification. *Automatica*, 46(1), 81–93.

Pillonetto, G., Dinuzzo, F., Chen, T., De Nicolao, G., and Ljung, L. (2014). Kernel methods in system identification, machine learning and function estimation: A survey. *Automatica*, 50(3), 657–682.

Rasmussen, C.E. and Williams, C.K.I. (2006). *Gaussian Processes for Machine Learning*. MIT Press Ltd.

Ryckaert, V.G., Claes, J.E., and Van Impe, J.F. (1999). Model-based temperature control in ovens. *J. Food Eng.*, 39(1), 47–58.

Scandella, M., Mazzoleni, M., Formentin, S., and Previdi, F. (2021). A Note on the Numerical Solutions of Kernel-Based Learning Problems. *IEEE Trans. Autom. Control*, 66(2), 940–947.

Scandella, M., Mazzoleni, M., Formentin, S., and Previdi, F. (2022). Kernel-based identification of asymptotically stable continuous-time linear dynamical systems. *Int. J. Control*, 95(6), 1668–1681.

Scandella, M., Moreschini, A., and Parisini, T. (2023). Kernel-Based Continuous-Time System Identification: A Parametric Approximation. In *Proc. 62nd IEEE Conf. Decis. Control*, 1492–1497.

Sidebotham, G. (2015). *Heat Transfer Modeling*. Springer.

Simard, J.D. and Moreschini, A. (2023). Enforcing Stability of Linear Interpolants in the Loewner Framework. *IEEE Control Syst. Lett.*, 7, 3537–3542.

Zhang, R., Xue, A., and Gao, F. (2014). Temperature control of industrial coke furnace using novel state space model predictive control. *IEEE trans. ind. inform.*, 10(4), 2084–2092.